Accepted Manuscript

Highly asymmetric hetero-Diels-Alder reaction using helical silica-supported Mn(III)-salen catalysts

Le Li, Yu Li, Di Pang, Fei Liu, Aqun Zheng, Guangbin Zhang, Yang Sun

Please cite this article as: Li L, Li Y, Pang D, Liu F, Zheng A, Zhang G, Sun Y, Highly asymmetric hetero-Diels-Alder reaction using helical silica-supported Mn(III)-salen catalysts, *Tetrahedron* (2015), doi: 10.1016/j.tet.2015.08.045.

Revised Graphical Abstract
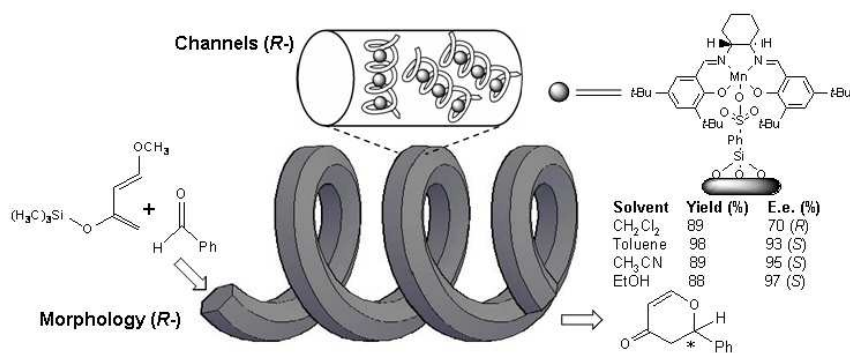
Highly asymmetric hetero-Diels-Alder reaction using helical silica-supported Mn(III)-salen catalysts

Le Li [a], Yu Li [a], Di Pang [b], Fei Liu [b], Aqun Zheng [a], Guangbin Zhang [c], Yang Sun [a,*]

[a] *Department of Applied Chemistry, School of Science, Xi'an Jiaotong University, No. 28, Xianning West Road, Xi'an 710049, PR China*

[b] *School of Materials & Chemical Engineering, Xi'an Technological University, No. 2, Xuefu Road, Xi'an 710021, PR China*

[c] *School of Pharmacy, Health Science Center, Xi'an Jiaotong University, No. 76, Yanta West Road, Xi'an 710061, PR China*

Abstract

Helical silica were prepared and functionalized by Mn(III)-salen complexes in order to catalyze asymmetric hetero-Diels-Alder reactions. Characterizations revealed doping of sodium lactate facilitated porosity, hydrolysis resistance and chiral configuration of silica matrix. Catalysis revealed the combination of Mn(III)-salen with helical silica had excellent chiral induction. Major product configuration was affected by temperature and solvent. Loading imidazolium ionic liquid as solvent improved both enantioselectivity and catalyst recycling.

Keywords: Helical silica; Mn(III)-salen; Immobilization; hetero-Diels-Alder.

1. Introduction

* Corresponding author. E-mail address: sunyang79@mail.xjtu.edu.cn (Y. Sun).

Asymmetric hetero-Diels-Alder (hDA) reaction of 1,3-diene with carbonyl compound provided a strategy for synthesis of chiral six-membered heterocycles, which had showed great values in both synthetic and pharmaceutical fields.[1,2] In view of reaction rate and scale, optical purity of product, as well as environmental protection, the application of efficient catalysts for hDA reaction had become an important selection for academic and industrial concerns.[3,4] Previously, metal complexes afforded excellent stereoselectivity and conversion for asymmetric hDA, including chromium-salen,[5] copper-Schiff-base,[6] titanium-binol,[7] zirconium-binol,[8] gold-phosphoramidite[9] or rare earth-phosphate[10]. Organocatalysts also attracted attentions due to avoidance of metal toxicity, tolerance of air, and convenient manipulation.[11] TADDOL (α,α,α',α'-tetraaryl-1,3-dioxolane-4,5-dimethanol),[12] oxazoline[13] or bis-sulfonamide[14] were typical examples. Even so, some key issues involving optical yield, catalyst recycling, cost of route and environmental burden still demanded endeavors for promotion.

Synthesis and application of chiral silica materials had aroused interests in recent years.[15] Immobilization of chiral metal complexes into chiral silica was an interesting alternative for heterogeneous asymmetric catalysis, because the synergy of two components might affect outputs, including conversion and stereoselectivity.[16] On the other hand, ionic liquids were chemically stable, non-volatile and nonflammable, but not very viscous.[17] Dispersion of metal catalysts into ionic liquid could avoid leaching of metal ions in some cases.[17] Therefore, ionic liquids were promising solvents in heterogeneous catalysis.[18]

In this work, a series of helical silica were prepared in a sol-gel procedure, where sodium lactate was doped in order to affect chirality. The Mn(III)-salen complexes (Jacobsen's catalyst) were immobilized into helical silica to catalyze asymmetric hDA reactions of Danishefsky's diene

with carbonyl compounds. In addition to regular solvents, two imidazolium ionic liquids BMImX ($BMIm^+$ = 1-*n*-butyl-3-methylimidazolium; X^- = NO_3^- or BF_4^-) were introduced to improve recycling of catalysts. Overall, this work would provide new chiral silica materials as well as an efficient catalytic system for asymmetric hDA reactions.

2. Results and discussion

2.1. Synthesis of catalysts

Synthesis of catalysts was shown in Scheme 1. Helical silica **N** was synthesized according to the method established by Ying and co-workers.[19] **L** and **D** were prepared according to the same process, except for the doping of chiral sodium lactate. Formation of helical silica would be discussed in Section 2.8.. Phenylsulfonylation of helical silica was performed according to literature with modifications.[20] At last, immobilization of Mn(III)-salen complexes into functional helical silica was performed in dichloromethane.
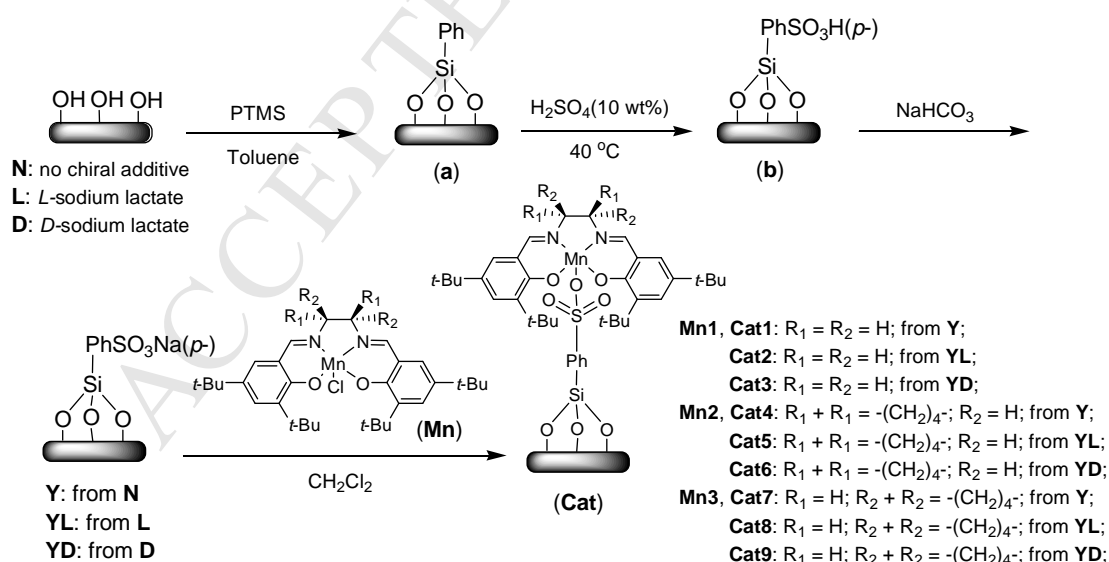
Scheme 1. Immobilization of Mn(III)-salen complexes into helical silica.
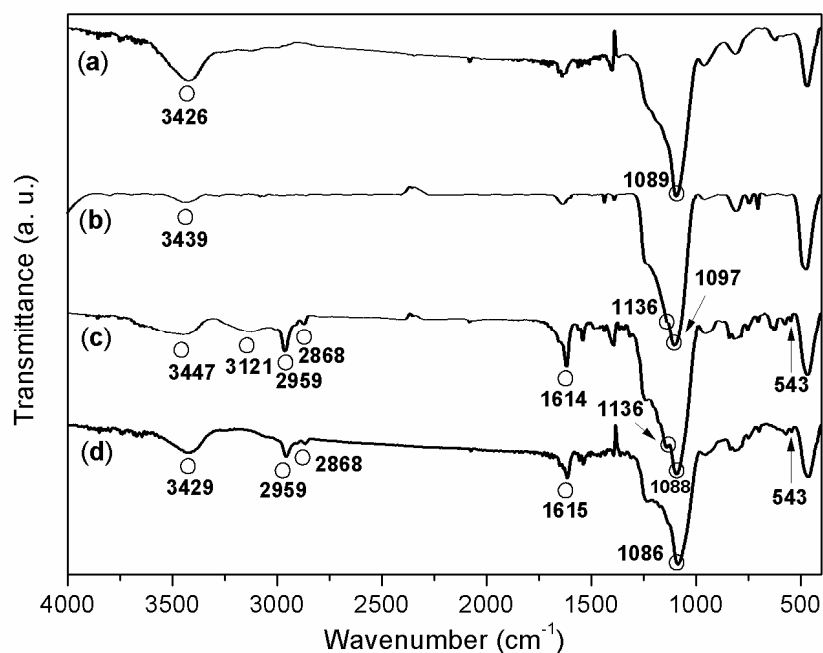
2.2. FT-IR study

Fig. 1. FT-IR of **L** (**a**), **YL** (**b**), **Cat5** (**c**) and **Cat6** (**d**).

Sample **L** showed the stretching vibration of SiO-H at 3426 cm^{-1}, which was sharply degraded and moved to 3439 cm^{-1} after functionalization, proving PTMS were attached to **L** (**a** *vs.* **b**, Fig. 1). Furthermore, the vibration at 1136 cm^{-1} represented anti-symmetric stretching of -SO$_3^-$, indicating phenylsulfonylation of **L** was available (**b**, Fig. 1).[21]

The 3447 cm^{-1} on **Cat5** could be ascribed to the stretching of non-substituted silanol groups, while 3121 cm^{-1} illustrated C-H stretching of benzene on **Mn2** (**c**, Fig. 1). Both 2959 and 2868 cm^{-1} characterized stretching of C-H on methyl. The 1614 cm^{-1} demonstrated C=N stretching, while a new peak at 543 cm^{-1} could be assigned to Mn-O stretching.[22] Although symmetric stretching of -SO$_3^-$ might be overlapped by Si-O stretching at 1088 cm^{-1}, the 1136 cm^{-1} still characterized anti-symmetric stretching of -SO$_3^-$ (**c**, Fig. 1).[21,22] All these data proved linkage of **Mn2** with **YL** was available.

There were no significant differences among **Cat4-6**, indicating sodium lactate would not change linking mode between Mn(III)-salen and helical silica (Fig. S1, Supplementary data; **c** and **d**, Fig. 1).

2.3. Nitrogen adsorption-desorption
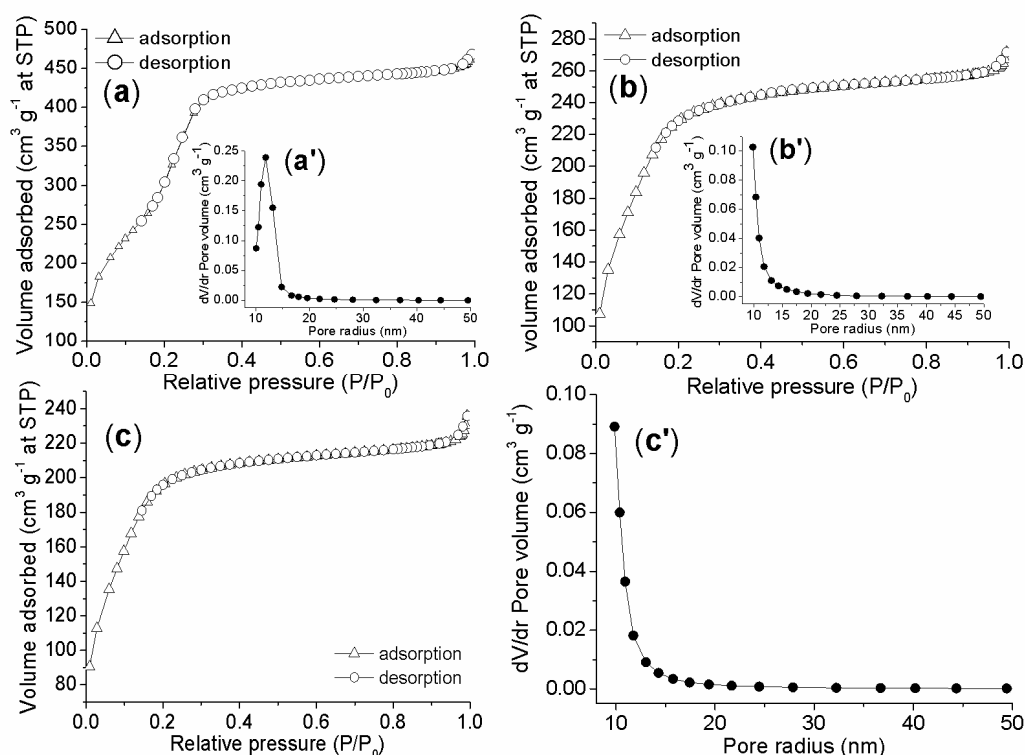
Fig. 2. Nitrogen adsorption-desorption isotherms and pore size distribution of **L** (**a** and **a'**), **YL** (**b** and **b'**) and **Cat6** (**c** and **c'**).

Both **N** and **L** showed type II isotherms, ordered pore size distributions, along with large surface areas, proving they had uniform channel-like mesopores (Fig. S2, Supplementary data; **a** and **a'**, Fig. 2; Table 1).[19,23] **L** showed larger BET surface area and pore volume than **N**, proving sodium lactate had unique template effects on porosity. Phenylsulfonylation of **L** decreased BET surface area and pore volume (**YL** *vs.* **L**, Table 1), but type of isotherms was basically preserved

(**b** *vs.* **a**, Fig. 2), indicating PTMS entered channels of **L**.

Immobilization of **Mn2** into **L** gave a poor porosity (**Cat5** *vs.* **L**, Table 1), so did that of **Mn2** into **Y** (**Cat4** *vs.* **N**, Table 1). However, attachment of **Mn2** to **D** showed a promising BET surface area (**Cat6** *vs.* **D**, Table 1), as well as type II isotherms and ordered pore size distribution (**c** and **c'**, Fig. 2). Therefore, the porous silica matrixes should be degraded to some extent during functionalization or immobilization.

Table 1

Textural parameters of samples

Sample	S_{BET}[a]	PV[b]	PR[c]	ρ[d]	d_S[e]	d_W[f]
N	958.2	6.4×10^{-1}	12.9	0.2	31.3	175.7
L	1372.9	8.6×10^{-1}	12.9	1.0	4.3	89.6
D	1190.7	7.5×10^{-1}	13.0	0.9	5.5	206.9
YL	770.6	2.2×10^{-1}	13.4	1.0	7.7	418.1
Cat5	59.3	6.8×10^{-2}	44.6	0.5	202.3	161.5
Cat4	20.0	7.6×10^{-2}	64.0	0.5	600.0	173.2
Cat6	660.8	1.9×10^{-1}	13.9	0.4	22.6	117.0

[a] Surface area ($m^2 g^{-1}$) determined by BET method based on N_2 adsorption.

[b] Pore volume ($cm^3 g^{-1}$), BJH method on N_2 adsorption.

[c] Pore radius (nm), BJH method on N_2 adsorption.

[d] Bulk density ($g cm^{-3}$).

[e] Crystallite size (nm) based on BET surface area: $d_S = 6/(S_{BET} \cdot \rho)$, ρ bulk density.

[f] Diameter of particle in CH_2Cl_2 (nm).
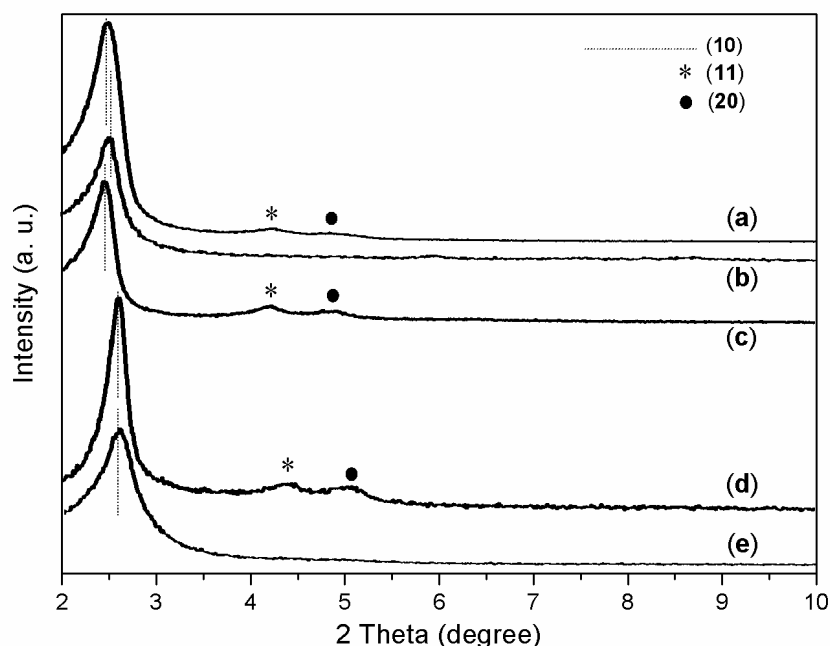
2.4. Low-angle X-ray diffraction

Fig. 3. Low-angle XRD of powdered **L** (**a**), **Cat5** (**b**), **D** (**c**), **YD** (**d**) and **Cat6** (**e**).

Both **N** and **L** as well as **D** showed hexagonal symmetry because 10, 11, 20 diffractions were detectable. Lattice constant (a) had an order as **N** (3.74 nm, $2\theta = 2.360^{\circ}$) > **D** (3.63 nm, $2\theta = 2.428^{\circ}$) > **L** (3.55 nm, $2\theta = 2.488^{\circ}$), which revealed doping of sodium lactate maintained hexagonal phase (Fig. S3, Supplementary data; Fig. 3).[19]

Attachment of PTMS and **Mn2** to **N** destroyed hexagonal symmetry completely (**b** *vs.* **a**, Fig. S3), but immobilizations of **L** and **D** looked much better, where only small diffractions such as 11 and 20 were degraded (**b** *vs.* **a**, **e** *vs.* **c**, Fig. 3), indicating doping of sodium lactate improved hydrolysis resistance of silica matrixes.[24] In particular, **YD** showed hexagonal symmetry similar to **D**, but had a narrower basal spacing (**d** *vs.* **c**, Fig. 3), demonstrating PTMS entered internal channels of **D** (Scheme 1). Furthermore, **YD** and **Cat6** shared an identical basal spacing of 3.40 nm at $2\theta = 2.596^{\circ}$ (**d** and **e**, Fig. 3), but 11 and 20 diffractions of **Cat6** disappeared, proving **Mn2** were mainly attached to 11 and 20 lattice planes of **YD** (**e** *vs.* **d**, Fig. 3).

7

2.5. X-ray photoelectron spectroscopy

Neither **N** nor **L** showed 1s photoelectron of nitrogen that demonstrated nitrogen-containing templates were completely removed after calcination (Table 2). Sodium lactate reduced content of carbon and doubled that of Si and O simultaneously, while binding energies were preserved, both proving sodium lactate accelerated removal of organic templates under calcination (**L** *vs.* **N**, Table 2).

After immobilization of PTMS and **Mn2** into **N**, contents and binding energies of Si and O on **N** were decreased, but content of carbon was increased, suggesting **Mn2** were attached to **N** (**Cat4** *vs.* **N**, Table 2). Similar tendency was found in variation of **L** to **Cat5**, and detection of sodium ions on **YL** proved salification was available (Table 2 and Scheme 1).

Table 2

Binding energy and atomic composition of Si, O, C, N and Mn on sample surface

Sample	Si (2p)	O (1s)	C (1s)	N (1s) / Na (1s)	Mn (2p)
N	104.0 (17.7)[a]	533.0 (26.7)	285.0 (55.2)	-	-
Cat4	103.0 (8.0)	532.0 (12.7)	285.0 (77.3)	399.0 (0.63)	642.0 (0.28)
L	104.0 (34.1)	533.0 (42.3)	285.0 (23.4)	-	-
YL	103.0 (31.3)	533.0 (35.4)	285.0 (33.1)	1072.0 (0.12)[b]	-
Cat5	103.0 (5.9)	532.0 (10.1)	285.0 (81.1)	399.0 (0.99)	642.0 (0.36)
Cat6	103.0 (27.6)	533.0 (31.3)	285.0 (40.6)	399.0 (0.16)	644.0 (0.11)

[a] Binding energy (eV), along with atomic percentage (at%) in parentheses.

[b] Above parameters of Na.

2.6. SEM and TEM
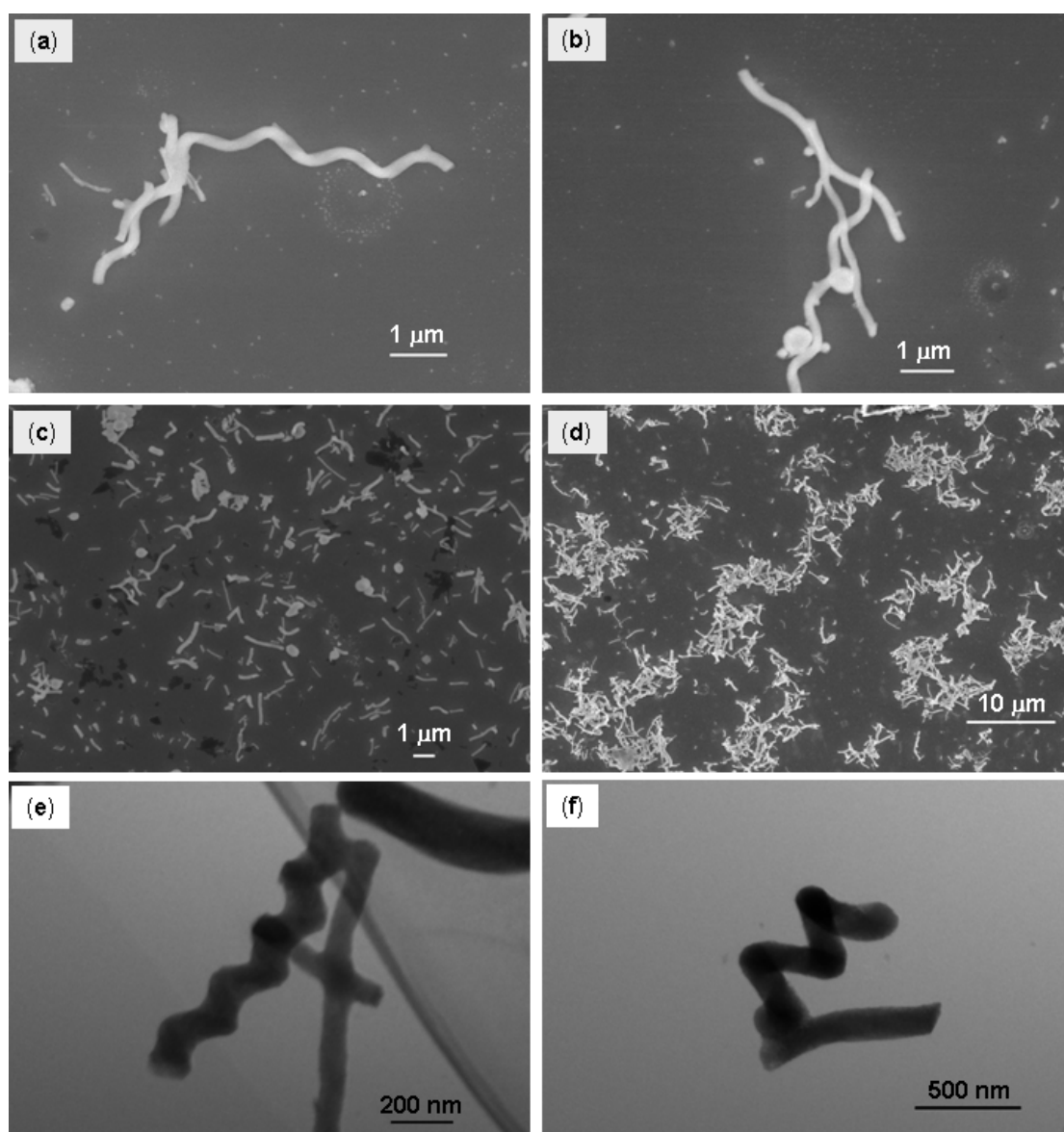
Fig. 4. SEM of **L** (**a**), **D** (**b**), **Cat5** (**c**), **Cat6** (**d**) and TEM of **Cat5** (**e**), **Cat6** (**f**).

The **N** was composed of helical rods having length of 0.5-5 μm, pitch of 0.5-1.5 μm, and offset (distance from spiral axis to center of rod) of 20-200 nm (**a"**, Fig. S4, Supplementary data). The **N** had both right- and left-handed morphologies, along with a small amount of amorphous blocks (**a"**, Fig. S4). Moreover, **L** and **D** showed the same appearance as **N** (**a**, **b**, Fig. 4; **b'**, **c'**, Fig. S4). Therefore, sodium lactate had little influences on morphology of helical silica.

Only phenylsulfonylation did not destroy morphology and porosity of helical silica (Scheme 1;

d' *vs.* **e'**, Fig. S4; **YL**, Table 1), but subsequent immobilization of **Mn2** degraded silica matrixes

sometimes. For example, **Cat4** was degraded into large sticky blocks (**f'** and **f''**, Fig. S4), which

was proved by a poor surface area (**Cat4**, Table 1). **Cat5** looked better owing to a small extent of

degradation (**c**, Fig. 4). **Cat6** appeared to be unaffected on appearance (**d**, Fig. 4), being approved

by a surface area of 660.8 m^2 g^{-1} (**Cat6**, Table 1). Thus, sodium lactate improved hydrolysis

resistance of helical silica. In addition, **Cat4**-**6** were all solid rods rather than hollow tubes based

on TEM observations (**f''**, Fig. S4; **e** and **f**, Fig. 4).

2.7. Configuration of internal channels

The **N** preferred *L*-valine rather than *D*-valine, but both **L** and **D** showed the contrary

adsorption priority, indicating channels of **N** were left-handed on average, while those of **L** and **D**

were right-handed (**b** and **c** *vs.* **a**, Fig. S5, Supplementary data).[25] **Y**, **YL** and **YD** had the same

chiral configuration as their precursors **N**, **L** and **D**, respectively (**d** *vs.* **a**, **e** *vs.* **b**, **f** *vs.* **c**, Fig. S5).

Meanwhile, adsorbed amount of **Y**, **YL** and **YD** were larger than **N**, **L** and **D**, mainly because

sodium benzene sulfonate groups had been fixed on silica surface (**d** *vs.* **a**, **e** *vs.* **b**, and **f** *vs.* **c**, Fig.

S5).

Cat4 maintained configuration of channels derived from **N** to **Y** (**g** *vs.* **d** and **a**, Fig. S5), but

Cat5 changed configuration of **YL** (**h** *vs.* **e**, Fig. S5), probably because Mn(III)-(*R*,*R*)salen (**Mn2**)

preferred *L*-valine more than *D*-valine, which might take effects on enantioselective adsorption

when content of Mn-salen units was high enough in catalyst (**Cat5**, Table S1, Supplementary data).

Accordingly, perhaps because **Cat6** had a lower Mn content than **Cat5** (Table S1),

enantioselective adsorption of valine on **Cat6** was still dominated by **YD** more than **Mn2** (**i** *vs.* **f**,

Fig. S5).

2.8. Proposed formation of helical silica
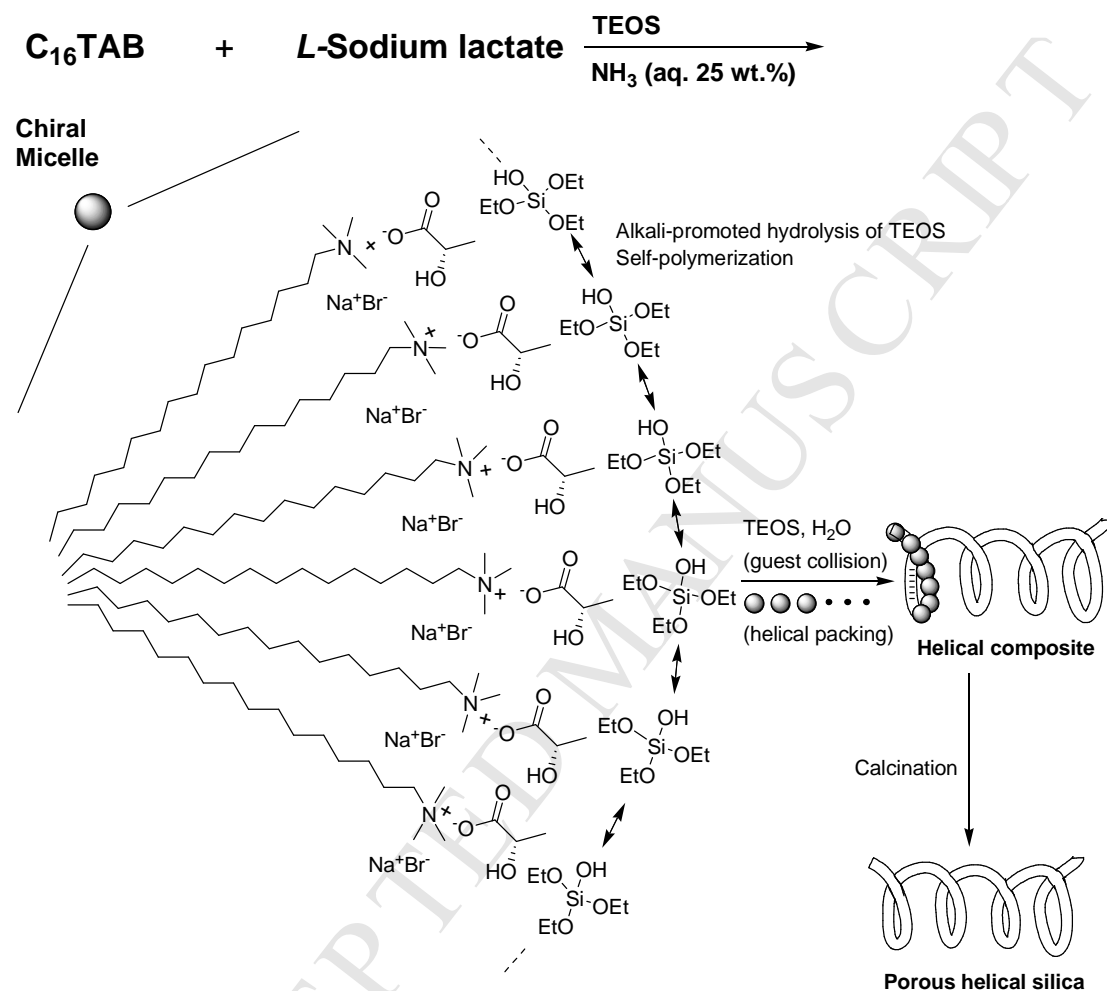
Fig. 5. Proposed formation of helical silica.

According to the above discussions, formation mechanism of helical silica was proposed in

Fig. 5. Herein, lactate anions would attract $C_{16}TAB$ cations that constructed framework of micelle.

Under alkaline environment, TEOS would be hydrolyzed and polymerized, providing shell and

stuff of micelle.

In view of a theory on entropy-driven formation of helices, a chain-like and flexible

macromolecule or agglomerate might be twisted in a crowded environment in order for maximum

entropy of guest molecules.[26] In this work, due to effects of entropy, packing of micelles would be twisted by collision of guest molecules such as TEOS and water, then be wrapped by self-polymerization of TEOS (Fig. 5).

Probably because collision of guest molecules was disordered, **N** and **L** as well as **D** had both left-handed and right-handed morphologies (Fig. 4 and Fig. S4). However, **N** was internally left-handed, while **L** and **D** were both right-handed (**a**, **b**, **c**, Fig. S5), proving chiral sodium lactate facilitated internal chirality of micelles in sol-gel (Fig. 5), and interestingly two enantiomers of sodium lactate had the same effects on internal configuration (**b** and **c**, Fig. S5).

2.9. Catalysis

Catalyst blank provided conversion of 3%, indicating molecular sieve (4Å) was catalytically active to some extent (entry 1, Table 3). **YL** showed conversion of 2 %, proving Mn(III)-salen would be catalytic center if positive results were obtained (entry 2). All other reactions proceeded smoothly during the entire work (Tables 3 and 4).
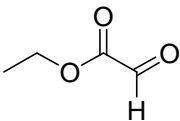
Because **Mn1** was achiral, asymmetric induction of **Cat1-3** depended on **Y**, **YL** and **YD** respectively (Scheme 1). **N** was left-handed (**a**, Fig. S5),[16] **L** and **D** were both right-handed (**b** and **c**, Fig. S5), but their combinations with **Mn1** showed good to excellent e.e. values for transformation of benzaldehyde (entries 3-5). Association of **L** with **Mn1** (**Cat2**) provided excellent e.e. for heptaldehyde too (entry 28). In addition, **Cat2** showed moderate to poor e.e. for acetophenone (entry 17), ethyl glyoxylate (entry 35) and cyclohexanecarboxaldehyde (entry 24). Therefore, chiral induction of helical silica was affirmative.

Table 3

Catalytic asymmetric hDA reactions of Danishefsky's diene with various carbonyl compounds

Entry[a]	Carbonyl	Catalyst	Solvent	T (°C)	Yield[b] (%)	E.e.[c] (%)	TOF[d] (h^{-1})
1		blank	CH_2Cl_2	0	3	0	-
2[a]		**YL**	CH_2Cl_2	0	2	0	-
3	PhCHO	**Cat1**	CH_2Cl_2	0	83	100 (S)	3.2
4		**Cat2**	CH_2Cl_2	0	65	100 (S)	5.4
5		**Cat3**	CH_2Cl_2	0	36	84 (S)	3.0
6		**Mn2**	CH_2Cl_2	0	40	45 (R)	3.3
7		**Cat4**	CH_2Cl_2	0	65	82 (R)	5.4
8		**Cat5**	CH_2Cl_2	0	94	57 (R)	7.9
9		**Cat5**	CH_2Cl_2	-78	79	73 (S)	6.6
10		**Cat6**	CH_2Cl_2	0	89	70 (R)	7.4
11		**Cat6**	toluene	0	98	93 (S)	8.2
12		**Cat6**	CH_3CN	0	89	95 (S)	7.4
13		**Cat6**	C_2H_5OH	0	88	97 (S)	7.4
14		**Cat7**	CH_2Cl_2	0	100	100 (S)	8.3
15		**Cat8**	CH_2Cl_2	0	100	91 (S)	8.3
16		**Cat9**	CH_2Cl_2	0	99	87 (S)	8.3
17		**Cat2**	CH_2Cl_2	0	77	-39	6.4
18		**Mn2**	CH_2Cl_2	0	36	25	3.0
19	$PhCOCH_3$	**Cat4**	CH_2Cl_2	0	81	-50	6.7
20		**Cat5**	CH_2Cl_2	0	90	58	7.5
21		**Cat5**	CH_2Cl_2	-78	66	-96	5.5
22		**Cat6**	CH_2Cl_2	0	83	48	6.9
23		**Cat7**	CH_2Cl_2	0	95	-67	7.9
24		**Cat2**	CH_2Cl_2	0	100	1 (R)	8.3
25		**Mn2**	CH_2Cl_2	0	100	29 (S)	8.3
26		**Cat5**	CH_2Cl_2	0	100	20 (S)	8.3
27		**Cat5**	CH_2Cl_2	-78	100	23 (R)	8.3
28		**Cat2**	CH_2Cl_2	0	89	-100	7.4
29		**Mn2**	CH_2Cl_2	0	100	56	8.3
30		**Cat4**	CH_2Cl_2	0	100	-10	8.3
31		**Cat5**	CH_2Cl_2	0	100	84	8.3
32		**Cat5**	CH_2Cl_2	-78	82	-95	6.8
33		**Cat6**	CH_2Cl_2	0	100	67	8.3
34		**Cat7**	CH_2Cl_2	0	100	-66	8.3

13

35		**Cat2**	CH_2Cl_2	0	100	-39	8.3
36		**Mn2**	CH_2Cl_2	0	66	77	5.5
37		**Cat4**	CH_2Cl_2	0	100	-59	8.3
38		**Cat5**	CH_2Cl_2	0	100	71	8.3
39		**Cat5**	CH_2Cl_2	-78	100	-98	8.3
40		**Cat6**	CH_2Cl_2	0	100	81	8.3
41		**Cat7**	CH_2Cl_2	0	100	-86	8.3

[a] Conditions same as in section 4.6.. Na of **YL** surface controlled at 2 mol% based on carbonyl substrate (Table 2).

[b] Molar percentage of hDA product to original carbonyl substrate, but those of entries 24-27 determined by diene.

[c] Enantiomeric excess. Retention time (min) for hDA product of benzaldehyde: 3.664 (*R*) and 4.040 (*S*), determined by comparison with literature[27]; product of acetophenone: 3.578 and 3.938, absolute configuration not determined, e.e. = ([early (retention time)] − [late]) / ([early] + [late]), also for other cases lack of absolute configurations; product of cyclohexanecarboxaldehyde[28]: 3.970 (*S*) and 6.197 (*R*); product of heptaldehyde[27]: 3.632 and 3.995, absolute configuration not determined; product of ethyl glyoxylate[29]: 3.621 and 3.970; absolute configuration not determined.

[d] Turnover frequency, $mol_{product} \, mol_{Mn}^{-1} \, (6 \, h)^{-1}$.

On the other hand, **Cat2** showed very high e.e. value for reaction of heptaldehyde, but showed very poor e.e. for cyclohexanecarboxaldehyde (entries 24 *vs.* 28). In the present system, the hydroxyl of silanol on **Cat2** would construct hydrogen bond in association with carbonyl substrate. Heptaldehyde has a long and flexible alkyl that could be induced by chiral centers on catalyst easily. However, the boat-to-chair conformation change of cyclohexyl on cyclohexanecarboxaldehyde could be restricted by silanols on **Cat2** through hydrogen-bond or other adsorptions, which might depress enantioselectivity. This phenomenon was different with those stemmed from strictly homogenous[27] or polymer-facilitated catalysis.[28]

Immobilization of **Mn2** into helical silica increased e.e. values, which were observed in

reactions of benzaldehyde (entries 7, 8, 10 *vs.* 6), acetophenone (entries 19, 20, 22 *vs.* 18), heptaldehyde (entries 31, 33 *vs.* 29) and ethyl glyoxylate (entries 40 *vs.* 36). On the other hand, **Mn2** dominated major configuration of hDA product of benzaldehyde rather than helical silica (entries 7 *vs.* 3; 8 *vs.* 4; 10 *vs.* 5), so did **Mn3** (entries 14 *vs.* 7, 15 *vs.* 8, 16 *vs.* 10). Similar trends were observed in transformations of acetophenone (entries 20 and 22 *vs.* 18; 23 *vs.* 19), cyclohexanecarboxaldehyde (entries 26 *vs.* 25), heptaldehyde (entries 31 and 33 *vs.* 29; 34 *vs.* 30) and ethyl glyoxylate (entries 38 and 40 *vs.* 36; 41 *vs.* 37). Therefore, Mn(III)-salen and helical silica had a synergy on chiral induction, where Mn(III)-salen controlled product configuration and helical silica took effects in promotion of e.e. values.

Combination of sodium lactate-doped silica (**YL** or **YD**) with **Mn2** afforded higher e.e. values than that of non-doped material (**Y**) for reactions of acetophenone (entries 20 *vs.* 19), heptaldehyde (entries 31 and 33 *vs.* 30) and ethyl glyoxylate (entries 38 and 40 *vs.* 37). Only a small deviation was observed in that of benzaldehyde (entries 8 and 10 *vs.* 7). Therefore, doping of sodium lactate improved chiral induction of helical silica.

The most significant result was temperature-facilitating major configuration of product, which was found in all substrates (entries 9 *vs.* 8; 21 *vs.* 20; 27 *vs.* 26; 32 *vs.* 31; 39 *vs.* 38). Herein, **Cat5** was composed of **YL** (mesoscopic chirality) and **Mn2** (molecular chirality), but they had contrary inducing direction on major configuration of product (entries 4 *vs.* 6). The 0 °C might provide a reaction of thermodynamic control where **Mn2** dominated configuration of product, but a much lower temperature (-78 °C) probably gave a kinetic control where **Mn2** and **YL** worked together.[30]
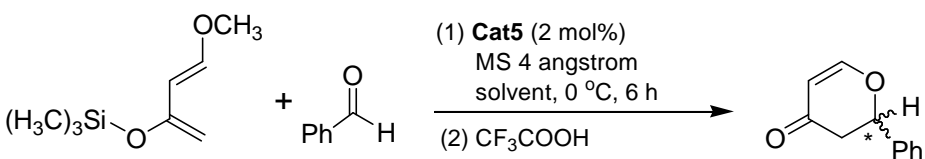
Another interesting phenomenon was effects of solvent on major configuration of product and enantioselectivity. In practice, toluene, acetonitrile and ethanol showed the same major

15

configuration in combination with **Cat6**, but dichloromethane gave different results (entries 11-13 *vs.* 10). Under **Cat5**, BMImNO$_3$ and BMImBF$_4$ showed a major configuration contrary to that from dichloromethane either (Table 4). Thus, the polarity of solvent, along with interaction of solvent with silica surfaces might play a key role in determination of major configuration of product. In addition, all polar solvents afforded satisfactory yields in transformation of benzaldehyde (entries 10-13). The stronger the polarity was, the higher the e.e. value was (entries 10 < 11 < 12 < 13 < ionic liquids of Table 4), indicating chiral induction of helical silica-supported Mn(III)-salen could be promoted under highly polarized media.[31]

2.10. Recycling of catalyst

Although fresh cycle achieved satisfactory yield and good enantioselectivity (entry 8), direct recycling of **Cat5** was not very efficient because no product was detected after four cycles (**Cat5**/CH$_2$Cl$_2$, Table 4). The weakening of Mn-O bond by valence change of Mn ion, or leaching of Mn(III)-salen complexes into *n*-hexane may take part in it (section 4.6.).[32]

In this work, BMImNO$_3$ and BMImBF$_4$ were employed as recycling media, and satisfactory e.e. values were obtained (Table 4). Obviously, two ionic liquids prevented degradation of Mn(III)-salen effectively, perhaps owing to coordination of nitrogen of imidazolyl into manganese ions. Furthermore, BMImBF$_4$ showed better yields than BMImNO$_3$ in recycling, probably because BF$_4^-$ showed higher affinity to Mn(III)-salen than NO$_3^-$ (Table 4). In practice, chemical modification of Jacobsen's catalyst could not always guarantee stereoselectivity.[33] However, this work provided a promising strategy for reusability of Mn(III)-salen catalyst without changing structure.

Table 4

Recycling of **Cat5** in imidazolium ionic liquids for hDA reaction of Danishefsky's diene with benzaldehyde

Catalyst	Yield (%), E.e. (%)[a]					
	Cycle fresh	Cycle 1	Cycle 2	Cycle 3	Cycle 4	Cycle 5
Cat5/CH$_2$Cl$_2$	94, 57 (R)[b]	80, 60 (R)	35, 25 (R)	10, 36 (R)	-	-
Cat5/BMImNO$_3$	88, 100 (S)	87, 100 (S)	80, 100 (S)	81, 100 (S)	70, 100 (S)	50, 100 (S)
Cat5/BMImBF$_4$	74, 100 (S)	77, 100 (S)	83, 100 (S)	70, 100 (S)	69, 100 (S)	74, 100 (S)

[a] Recycling details same as in section 4.6., other parameters same as in Table 3.

[b] Entry 8, Table 3.

3. Conclusions

In conclusion, doping of sodium lactate significantly changed porosity, internal configuration and hydrolysis resistance of helical silica. In heterogeneous catalysis, combination of achiral Mn(III)-salen complex with helical silica provided high enantioselectivity, while the synergy of Mn(III)-salen with helical silica on chiral induction was present. Secondly, temperature and solvent showed important influences on major configuration of products as well as enantioselectivity. At last, imidazolium ionic liquids were efficient media for recycling of catalyst. This work developed a new series of chiral silica materials, and provided a highly asymmetric, recyclable, green and low-cost route to catalytic asymmetric hetero-Diels-Alder reaction.

4. Experimental

4.1. Starting materials

Hexadecyltrimethylammonium bromide (C$_{16}$TAB), tetraethyl orthosilicate (TEOS), *L*- and

D-sodium lactate, ammonia solution (25 wt.%), phenyltrimethoxysilane (PTMS), Danishefsky's

diene (1-methoxy-3-trimethylsilyloxy-1,3-butadiene, 94 wt.%), benzaldehyde, acetophenone,

cyclohexanecarboxaldehyde, heptaldehyde, ethyl glyoxylate (50 wt.% in toluene) and

trifluoroacetic acid were purchased from Aldrich, Accela or Acros. Jacobsen's catalyst (**Mn1-3**,

Scheme 1; Sections 1-2, Supplementary data),[34] and ionic liquid BMImX (BMIm$^+$ =

1-*n*-butyl-3-methylimidazolium; X$^-$ = BF$_4$$^-$)[35] were synthesized according to literatures (Section 4,

Supplementary data). BMImX (X$^-$ = NO$_3$$^-$) was prepared by the ion-exchanging of commercial

BMImCl with AgNO$_3$ in distilled water (Section 3, Supplementary data).

4.2. Instruments

^{1}H NMR was recorded on Bruker ADVANCE III (400MHz). ESI-HRMS was detected on

microOTOF-Q II, Bruker.Daltonics. GC-MS was carried out on GCMS-QP2010 Plus, Shimadzu.

Mn contents were measured by inductively coupled plasma atomic emission spectrometry

(ICP-AES) on ICPE-9000, Shimadzu. FT-IR was reported in KBr pellets on Bruker Tensor 27,

with wave numbers of 400-4000 cm^{-1}.

BET surface area, pore volume, pore radius and pore size distribution were performed on

Micromeritics ASAP 2020, using N$_2$ adsorption isotherms at 77.35 K. Samples were degassed at

150 ^{o}C in vacuum before testing. Surface area was calculated on these isotherms using the

multi-point Brunauer-Emmett-Teller (BET) method based on adsorption data in relative pressure

P/P_0 of 0.06-0.3. Total pore volume was obtained from N$_2$ adsorbed at P/P_0 = 0.97. Pore volume

and pore radius were determined using Barrett-Joyner-Halenda (BJH) method.

Particle size was tested in CH$_2$Cl$_2$ at 298 K on Zetasizer Nano ZS90, Malvern. Low-angle

X-ray diffractions (2θ at 0.5^o to 10°) of powdered samples were reported on Philips X'Pert Pro diffractometer using Cu-Ka radiation (λ, 1.5418 Å), with interval of 0.05^o second^{-1}, scattering signals of 0.5^o-2.0^o were omitted for clarity. X-ray photoelectron spectroscopy (XPS) was carried out on Kratos Axis Ultra DLD, using monochromatic Al Kα X-ray (1486.6 eV) as irradiation source, the binding energy scale was calibrated by using C 1s peak at 285.0 eV. Scanning electron microscopy (SEM) was performed on JEOL JSM-6700F at 20.0 kV with Au coating. Transmission electron microscopy (TEM) was tested on JEOL JEM-200CX at 120 kV.

Internal chirality of samples was characterized by enantioselective adsorption of valine in water.[25] In practice, sample (20 mg) and *L*-(or *D*-)valine (50 mg) were added to distilled water (20 mL), then stirred at 25 ^{o}C for 120 minutes. Concentration of *L*-(or *D*-)valine was monitored at regular intervals by UV (210 nm, UV 1800, Shimadzu). Adsorption percentage was determined by Lambert-Beer's Law, then plotted as a function of time.

Thin layer chromatography (TLC) was performed on glass plates coated with GF$_{254}$ silica gel, with coloration in phosphomolybdic acid (PMA)/ethanol solution (5 wt.%). Yield and e.e. were determined by HPLC (Section 12, Supplementary data). System controller: Waters 1525, binary hplc pump; UV-Vis detector: Waters 2998, photodiode array detector; UV: 254 nm for 2,3-dihydro-2-phenyl-4*H*-pyran-4-one   (from   benzaldehyde), 2,3-dihydro-2-methyl-2-phenyl-4*H*-pyran-4-one   (acetophenone), 2-cyclohexyl-2,3-dihydro-4*H*-pyran-4-one   (cyclohexanecarboxaldehyde), 2-hexyl-2,3-dihydro-4*H*-pyran-4-one   (heptaldehyde)   and 2-ethoxyformyl-2,3-dihydro-4*H*-pyran-4-one (ethyl glyoxylate), obtained by scanning 200-400 nm. Daicel Chiralcel OD-H, size: 150 mm $\times$ 4.6 mm; particle: 5 μm; mobile phase:

n-hexane/2-propanol, 90/10, v/v; rate: 0.5 mL min^{-1}; column temperature: 300 K, pressure: 3.0-3.5

MPa; sample concentration: 0.5 mg mL^{-1} in *n*-hexane; injection: 10 μL.

4.3. Synthesis of helical silica

Sample **N** was synthesized according to literature.[19] **L** and **D** were prepared as follows.

C$_{16}$TAB (0.40 g, 1.09 mmol) and *L*-(or *D*-)sodium lactate (0.06 g, 0.54 mmol) were dissolved in

aqueous ammonia (25 wt.%, 100 mL) at 40 $^{\circ}$C. TEOS (2.0 mL, 1.86 g, 8.95 mmol) was

introduced. The mixture was slowly stirred (800 rpm) at 40 $^{\circ}$C for 3 h, then aged at 100 $^{\circ}$C for 24

h in autoclave. White solids (**L** or **D**) were filtered, dried in air, calcined at 550 $^{\circ}$C for 5 h to

remove templates.

4.4. Phenylsulfonylation of helical silica

N (**L** or **D**, 0.9 g) was dehydrated at 60 $^{\circ}$C for 24 h, then added to dry toluene (150 mL), and

dispersed by ultrasound at 25 $^{\circ}$C for 3 h. PTMS (2.1 mL, 2.2 g, 11.3 mmol) was introduced. The

mixture was stirred at 25 $^{\circ}$C for 1 h, then refluxed at 120 $^{\circ}$C for 18 h. After being cooled to 25 $^{\circ}$C,

compound **a** was filtered, washed with ethanol (3×20 mL), dried at 60 $^{\circ}$C for 12 h.

The **a** (3.0 g) was added to H$_2$SO$_4$ (10 wt.%, 10 mL), then stirred at 40 $^{\circ}$C for 2 h. The

resulting **b** was filtered and washed with water until pH was 7, further with ethanol (3×20 mL),

dried in air. Next, NaHCO$_3$ solution (0.195 mol L^{-1}, 20 mL) was added, stirred for 3 h at 25 $^{\circ}$C. **Y**

(**YL** or **YD**) was filtered, washed to neutral with water, dried in air.

4.5. Synthesis of helical silica-supported Mn(III)-salen complexes

Mn1 (**-2**, **-3**; 100 mg) and **Y** (**YL**, **YD**; 300 mg) were added to dichloromethane (20 mL), then stirred at 40 °C for 3 h. The solids were collected by filtration and washed by distilled water (3×30 mL) and ethanol (3×30 mL), then dried in air.

4.6. Catalytic asymmetric hetero-Diels-Alder reaction

Carbonyl compound (1.0 mmol), Danishefsky's diene (1.0 mmol), molecular sieve (50 mg, 4Å) and catalyst (2 mol% Mn based on carbonyl) were added to solvent (including ionic liquid, 3.0 mL), then stirred at 0 °C (or at -78 °C, in Dewar bottle of 250 mL, filled with liquid nitrogen and acetone), and monitored by TLC/PMA (petroleum ether; R_f of Danishefsky's diene: 0.3; R_f of benzaldehyde, acetophenone, cyclohexanecarboxaldehyde, heptaldehyde, ethyl glyoxylate,: 0.48, 0.43, invisible, 0.5, 0.64; R_f of above hDA products: 0.56, 0.87, 0.71, 0.72, 0.70, accordingly). The hDA products were further characterized by ^{1}H NMR and mass spectra (Section 11, Supplementary data). After 6 h, trifluoroacetic acid (50 μL) was added and stirred for 1 h. Mixture was concentrated, extracted by *n*-hexane (3×5 mL), the left catalyst (including ionic liquid layer) was reloaded with consumables for recycling. Hexane layer was concentrated. The crude product was purified by flash chromatography (SiO₂, 200-300 mesh, pure petroleum ether), then tested on chiral HPLC (Section 12, Supplementary data).

Helical Materials in Catalytic Asymmetric Reactions).

Supplementary data

Complementary characterizations of synthetic samples and templates of chiral HPLC.

References and notes

1.   Pellissier, H. *Tetrahedron* **2009**, *65*, 2839.

2.   Gaunt, M. J.; Johansson, C. C. C.; McNally, A.; Vo, N. T. *Drug Discov. Today* **2007**, *12*, 8.

3.   Lanari, D.; Montanari, F.; Marmottini, F.; Piermatti, O.; Orrù, M.; Vaccaro, L. *J. Catal.* **2011**, *277*, 80.

4.   Zhao, B.; Loh, T. *Org. Lett.* **2013**, *15*, 2914.

5.   Schaus, S. E.; Brånalt, J.; Jacobsen, E. N. *J. Org. Chem.* **1998**, *63*, 403.

6.   Lin, L.; Fan, Q.; Qin, B.; Feng, X. *J. Org. Chem.* **2006**, *71*, 4141.

7.   Long, J.; Hu, J.; Shen, X.; Ji, B.; Ding, K. *J. Am. Chem. Soc.* **2002**, *124*, 10.

8.   Yamashita, Y.; Saito, S.; Ishitani, H.; Kobayashi, S. *Org. Lett.* **2002**, *4*, 1221.

9.   Liu, B.; Li, K. -N.; Luo, S. -W.; Huang, J. -Z.; Pang, H.; Gong, L. -Z. *J. Am. Chem. Soc.* **2013**, *135*, 3323.

10. Furuno, H.; Hayano, T.; Kambara, T.; Sugimoto, Y.; Hanamoto, T.; Tanaka, Y.; Jin, Y. Z.; Kagawa, T.; Inanaga, J. *Tetrahedron* **2003**, *59*, 10509.

11. Chatelet, B.; Dufaud, V.; Dutasta, J.-P.; Martinez, A. *J. Org. Chem.* **2014**, *79*, 8684.

12. Huang, Y.; Unni, A. K.; Thadani, A. N.; Rawal, V. H. *Nature* **2003**, *424*, 146.

13. Rajaram, S.; Sigman, M. S. *Org. Lett.* **2005**, *7*, 5473.

14. Zhuang, W.; Poulsen, T. B.; Jøgensen, K. A. Org. Biomol. Chem. **2005**, *3*, 3284.

15. Che, S.; Liu, Z.; Ohsuna, T.; Sakamoto, K.; Terasaki, O.; Tatsumi, T. *Nature* **2004**, *429*, 281.

16. Fernandes, C. I.; Saraiva, M. S.; Nunes, T. G.; Vaz, P. D.; Nunes, C. D. *J. Catal.* **2014**, *309*, 21.

17. Gu, Y.; Li, G. *Adv. Synth. Catal.* **2009**, *351*, 817.

18. Jin, X.; Xu, X.; Zhao, K. *Tetrahedron: Asymmetry* **2012**, *23*, 1058.

19. Han, Y.; Zhao, L.; Ying, J.Y. *Adv. Mater.* **2007**, *19*, 2454.

20. Zhang, H.; Zhang, Y.; Li, C. *J. Catal.* **2006**, *238*, 369.

21. Choudary, B. M.; Ramani, T.; Maheswaran, H.; Prashant, L.; Ranganath, K. V. S.; Kumar, K. V. *Adv. Synth. Catal.* **2006**, *348*, 493.

22. Zhang, Z.; Guan, F.; Huang, X.; Wang, Y.; Sun, Y. *J. Mol. Catal. A: Chem.* **2012**, *363-364*, 343.

23. Sing, K. S. W.; Everett, D. H.; Haul, R. A. W.; Moscou, L.; Pierotti, R. A.; Rouquérol, J.; Siemieniewska, T. *Pure Appl. Chem.* **1985**, *57*, 603.

24. Galarneau, A.; Nader, M.; Guenneau, F.; Renzo, F. D.; Gedeon, A. *J. Phys. Chem. C* **2007**, *111*, 8268.

25. Guo, Z.; Du, Y.; Chen, Y.; Ng, S. -C.; Yang, Y. *J. Phys. Chem. C* **2010**, *114*, 14353.

26. Snir, Y.; Kamien, R. D. *Science* **2005**, *307*, 1067.

27. Aikawa, K.; Irie, R.; Katsuki, T. *Tetrahedron* **2001**, *57*, 845.

28. Mellah, M.; Ansel, B.; Patureau, F.; Voituriez, A.; Schulz, E. *J. Mol. Catal. A: Chem.* **2007**, *272*, 20.

29. Motoyama, Y.; Koga, Y.; Nishiyama, H. *Tetrahedron* **2001**, *57*, 853.

30. Li, H. -B.; Page, A. J.; Irle, S.; Morokuma, K. *J. Phys. Chem. Lett.* **2013**, *4*, 3176.

31. Leach, A. G.; Houk, K. N. *J. Org. Chem.* **2001**, *66*, 5192.

32. Hoffmann, F.; Cornelius, M.; Morell, J.; Fröba, M. *Angew. Chem. Int. Ed.* **2006**, *45*, 3216.

33. Zulauf, A.; Mellah, M.; Hong, X.; Schulz, E. *J. Chem. Soc., Dalton Trans.* **2010**, *39*, 6911.

34. Larrow, J. F.; Jacobsen, E. N.; Gao, Y.; Hong, Y.; Nie, X.; Zepp, C. M. *J. Org. Chem.* **1994**, *59*, 1939.

35. Suarez, P. A. Z.; Dullius, J. E. L.; Einloft, S.; De Souza, R. F.; Dupont, J. *Polyhedron* **1996**, *15*, 1217.